

Alma Mater Studiorum Università di Bologna  
Archivio istituzionale della ricerca

(9R)-9-Hydroxystearate-Functionalized Hydroxyapatite as Antiproliferative and Cytotoxic Agent toward Osteosarcoma Cells.

This is the final peer-reviewed author's accepted manuscript (postprint) of the following publication:

*Published Version:*

Elisa Boanini, Paola Torricelli, Carla Boga, Gabriele Micheletti, Maria Cristina Cassani, Milena Fini, et al. (2016). (9R)-9-Hydroxystearate-Functionalized Hydroxyapatite as Antiproliferative and Cytotoxic Agent toward Osteosarcoma Cells. *LANGMUIR*, 32(1), 188-194 [10.1021/acs.langmuir.5b03754].

*Availability:*

This version is available at: <https://hdl.handle.net/11585/533887> since: 2020-02-24

*Published:*

DOI: <http://doi.org/10.1021/acs.langmuir.5b03754>

*Terms of use:*

Some rights reserved. The terms and conditions for the reuse of this version of the manuscript are specified in the publishing policy. For all terms of use and more information see the publisher's website.

This item was downloaded from IRIS Università di Bologna (<https://cris.unibo.it/>).  
When citing, please refer to the published version.

(Article begins on next page)

This is the final peer-reviewed accepted manuscript of:

Elisa Boanini, Paola Torricelli, Carla Boga, Gabriele Micheletti, Maria Cristina Cassani, Milena Fini, and Adriana Bigi; “(9*R*)-9-Hydroxystearate-Functionalized Hydroxyapatite as Antiproliferative and Cytotoxic Agent toward Osteosarcoma Cells” (2016) *Langmuir* 32: 188–194. [doi.org/10.1021/acs.langmuir.5b03754](https://doi.org/10.1021/acs.langmuir.5b03754)

The final published version is available online at:  
<https://pubs.acs.org/doi/10.1021/acs.langmuir.5b03754>

#### Rights / License:

The terms and conditions for the reuse of this version of the manuscript are specified in the publishing policy. For all terms of use and more information see the publisher's website.

*This item was downloaded from IRIS Università di Bologna (<https://cris.unibo.it/>)*

***When citing, please refer to the published version.***

# **(9*R*)-9-Hydroxystearate-Functionalized Hydroxyapatite as Anti-Proliferative and Cytotoxic Agent towards Osteosarcoma Cells.**

Elisa Boanini,<sup>1\*</sup> Paola Torricelli,<sup>2</sup> Carla Boga,<sup>3\*</sup> Gabriele Micheletti,<sup>3</sup> Maria Cristina Cassani,<sup>3</sup>  
Milena Fini <sup>2</sup> and Adriana Bigi<sup>1</sup>

<sup>1</sup> Department of Chemistry “G. Ciamician”, via Selmi 2, University of Bologna, 40126 Bologna, Italy

<sup>2</sup> Laboratory of preclinical and surgical studies, Research Institute Codivilla Putti – Rizzoli Orthopaedic Institute, via di Barbiano, 40136 Bologna, Italy

<sup>3</sup> Department of Industrial Chemistry “Toso Montanari”, Viale del Risorgimento 4, University of Bologna, 40136 Bologna, Italy

Corresponding Authors:

\*Dr. Elisa Boanini      e-mail: elisa.boanini@unibo.it

\*Dr. Carla Boga      e-mail: carla.boga@unibo.it

**ABSTRACT:** The possibility to functionalize calcium phosphates with bioactive agents is a promising strategy to design innovative biomaterials for bone repair able to couple the bioactive properties of the inorganic compounds with the therapeutic effect of the functionalizing agent. The R enantiomer of the 9-hydroxystearic acid, (9*R*)-9-HSA, produced from *Dimorphotheca sinuata* L. seeds, has proven to act as a natural negative regulator of tumor cell proliferation. On this basis, hydroxyapatite was synthesized with increasing contents of (9*R*)-9-hydroxystearate, up to about 8.6 wt%. The incorporation of HSA in the composite nanocrystals induces a reduction of the crystal mean dimensions and of the length of the coherently scattering crystalline domains, which suggest a preferential adsorption onto the hydroxyapatite crystal faces parallel to the *c*-axis direction. The composite nanocrystals were designed so that their cytostatic and cytotoxic effects towards osteosarcoma cells are modulated by hydroxystearate content. In fact, results of in vitro tests show that the presence of HSA in the composite nanocrystals provokes a significant decrease of SaOS2 osteosarcoma cells proliferation and viability, as well as an increase of Lactate Dehydrogenase, Tumor Necrosis Factor  $\alpha$ , and Caspase 3 levels, with a cytotoxic effect increasing with HSA content in the nanocrystals.

**Keywords:** hydroxyapatite, hydroxystearic acid, osteosarcoma, nanocrystals, citotoxicity, bone repair

## 1. Introduction

Musculoskeletal disorders, such as osteoporosis, osteoarthritis, bone tumors, cause decreased life quality and enormous economic loads on National Health Services worldwide. The problem requires

innovative biomaterials able not only to integrate with host tissue and promote new bone formation, but also to provide bioactive molecules potentially useful to counteract specific metabolic disorders. Calcium phosphates are widely used for the preparation of biomaterials for hard tissues substitution/repair not only as fillers and coatings, but also for the preparation of bone cements and composite scaffolds.<sup>1-4</sup> As a matter of fact, these compounds exhibit an excellent biocompatibility and bioactivity. From a chemical and structural point of view, hydroxyapatite (HA) is the calcium phosphate most similar to the mineral component of bones and teeth, which justifies its huge amount of applications in the biomedical field. HA functionalization with bioactive ions, molecules and drugs has proven to be a successful strategy to couple the beneficial effect of the calcium phosphate on promotion of new bone formation with the specific action of the functionalizing agent.<sup>5-8</sup>

9-Hydroxystearic acid (9-HSA) is a long-chain monohydroxy fatty acid belonging to the class of endogenous lipid peroxidation by-products and plays an important role as natural negative regulator of tumor cell proliferation. Its content strongly diminishes in tumor cells, causing the loss of one of the control mechanisms on cell division.<sup>9</sup>

9-HSA acts as inhibitor of histone deacetylase (HDAC), an enzymatic family that is considered a potential target for antitumor therapies.<sup>10</sup> Its administration to HT29, a human colon adenocarcinoma cell line, induced a control of the cell growth and differentiation by inhibiting HDAC1 activity through a direct fatty acid/enzyme interaction.<sup>10,11</sup>

Its administration to U2OS, an osteosarcoma cell line, provoked a growth arrest of the cells in G2/M cycle and apoptosis via a mitochondrial pathway.<sup>12</sup> Moreover, molecular docking indicated a favorable formation energy of the HDAC1-9-HSA complex and a higher stability of bonding for the enantiomer (9*R*)-9-HSA with respect to that with opposite configuration.<sup>10</sup> This prediction was confirmed by administering (9*R*)-9-HSA and (9*S*)-9-HSA to HT-29 cells.<sup>13</sup> To this aim, the synthesis of the two enantiomers in almost pure form was realized starting from *Dimorphoteca sinuata* L. seeds, containing a natural precursor bearing the hydroxyl functionality on the enantiomerically pure chiral center in position 9.<sup>14</sup> At variance, classical

enantioselective synthetic methods or kinetic resolution methods revealed to be not successful for the synthesis of the two acids in enantiomerically pure form, due to the high symmetry around the chiral center of these compounds.<sup>15</sup>

In this work, we explored the possibility to functionalize HA with HSA with the objective to obtain composite nanocrystals with modulated cytotoxic effect on cancer cells. To this aim, we synthesized HA in the presence of increasing concentrations of potassium (9*R*)-9-hydroxystearate (9*R*-HSA-K), which was chosen because of its greater water solubility than (9*R*)-9-HSA. The products were submitted to a detailed structural, morphological and chemical characterization in order to investigate the interaction between HA and the drug. In vitro tests carried out using an osteosarcoma cell line (SaOS2) show that the composite nanocrystals exhibit a cytostatic and cytotoxic effect related to hydroxystearate content.

## 2. Experimental Section

### 2.1 Synthesis and characterization of potassium (9*R*)-9-hydroxystearate

Potassium (9*R*)-9-hydroxystearate was obtained by salification of (9*R*)-9-hydroxystearic acid, prepared starting from *Dimorphotheca sinuata* L. seeds as described in Supporting Information, where detailed information on materials and methods used are also included.

(9*R*)-9-hydroxystearic acid was dissolved in a 5% w/v methanolic solution of KOH, so that KOH is equimolar with the acid. The solution was stirred for 3h. The reaction was monitored by thin layer chromatography (TLC) and once completed the methanol was removed under vacuum. The light yellow solid obtained was dissolved in 10 mL of boiling water and left to cool to room temperature. The precipitate, if present, was filtered off and, after removal of the water by heating at 45 °C under vacuum, potassium (9*R*)-9-hydroxystearate was recovered as a light yellow powder. <sup>1</sup>H NMR (399.9 MHz, D<sub>2</sub>O): 3.44–3.35 (m, 1H, CHOH), 1.98 (t, *J* = 7.7Hz, 2H, CH<sub>2</sub>COO), 1.36 (quint, *J* = 6.9Hz, 2H, CH<sub>2</sub>CH<sub>2</sub>COO), 1.32–1.02 (m, 27 H incl. OH), 0.69 (t, *J* = 7.0Hz, 3H, CH<sub>3</sub>). IR (KBr): 1558 cm<sup>-1</sup>. ESI-MS (ES<sup>-</sup>): *m/z* = 299 [M – H]<sup>-</sup>.

## 2.2 Synthesis and characterization of composite samples

The synthesis of hydroxyapatite was carried out in N<sub>2</sub> atmosphere using 50 mL of 0.65 M (NH<sub>4</sub>)<sub>2</sub>HPO<sub>4</sub> solution at pH adjusted to 10 with NH<sub>4</sub>OH. The solution was heated at 90 °C and 50 mL of 1.08 M Ca(NO<sub>3</sub>)<sub>2</sub>·4 H<sub>2</sub>O solution, pH 10 adjusted with NH<sub>4</sub>OH, was added drop-wise under stirring. The precipitate was maintained in contact with the reaction solution for 5 h at 90 °C under stirring, then centrifuged at 10,000 rpm for 10 min and repeatedly washed with CO<sub>2</sub>-free distilled water. The product was dried at 37 °C overnight.

Samples containing HSA were obtained by adding potassium (9*R*)-9-hydroxystearate to the phosphate solution prior to the addition of calcium nitrate tetrahydrate. The concentrations of potassium (9*R*)-9-hydroxystearate used were 5, 10, 15 and 20 mM, calculated on final volume. The resulting solid samples were labeled as HAHSA5, HAHSA10, HAHSA15, HAHSA20, where digits indicate the concentration of potassium (9*R*)-9-hydroxystearate used in the specific preparation.

The traditional direct synthesis of hydroxyapatite is usually done with the slow addition of (NH<sub>4</sub>)<sub>2</sub>HPO<sub>4</sub> onto Ca(NO<sub>3</sub>)<sub>2</sub>·4 H<sub>2</sub>O.<sup>16</sup> Soluble 9*R*-HSA-K has an anionic behavior and should be added to the ammonium phosphate solution so that it is slowly put into contact with the calcium ions. Initially this method was tested, but proved to be unfeasible due to the precipitation of 9*R*-HSA-K in the addition funnel. This problem was solved by heating ammonium phosphate and 9*R*-HSA-K until the solution was homogeneous, and then adding calcium nitrate drop-wise. The addition of calcium nitrate started only after the complete dissolution of 9*R*-HSA-K.

The chemical, structural and morphological properties of the samples were investigated as reported in the Supporting Information.

*In vitro* tests were performed on disk-shaped samples (Ø= 6.0 mm). Each disk was prepared by pressing 40 mg of powder into cylindrical moulds by using a standard evacuable pellet die (Hellma), and sterilized using gamma rays (Cobalt-60) at a dose of 25 kGy.

## 2.3 *In vitro* studies

SaOS-2 osteosarcoma cell line was expanded in DMEM low glucose medium (Sigma, UK) supplemented with 10% FCS, and antibiotics (100 U/ml penicillin, 100 µg/ml streptomycin). Cells were detached from culture flasks by trypsinization, and cell number and viability were checked by trypan blue dye exclusion test. Cells were plated at a density of  $2 \times 10^4$  cells/mL in 12-well plates onto sterile samples synthesized at four different concentrations of HSA (HAHSA5, HAHSA10, HAHSA15, HAHSA20), of HA as reference, and in wells for negative (CTR–, DMEM only) and positive (CTR+, DMEM + 0.05% phenol solution) controls for cytotoxicity tests, according to UNI EN ISO 10993-5.<sup>17</sup> Plates were cultured in standard conditions, at  $37 \pm 0.5^\circ\text{C}$  with 95% humidity and  $5\% \pm 0.2 \text{ CO}_2$ .

### *2.3.1 Cytotoxicity tests*

Cytotoxicity tests were performed after 3 days of culture.<sup>17</sup> Cell proliferation and viability was assessed by WST1 (WST1, Roche Diagnostics GmbH, Mannheim, Germany) colorimetric reagent test. The assay is based on the reduction of tetrazolium salt to a soluble formazan salt by a reductase of the mitochondrial respiratory chain, active only in viable cells. 100 µl of WST1 solution and 900 µl of medium (final dilution: 1:10) were added to the cell monolayer, and the multi-well plates were incubated at  $37^\circ\text{C}$  for a further 4 h. Supernatants were quantified spectrophotometrically at 450 nm with a reference wavelength of 625 nm. Results of WST1 are reported as optical density (OD) and directly correlate with the cell number.

At the end of experimental time the supernatant was collected from all wells to detect Lactate Dehydrogenase (LDH, enzyme-kinetic test, Roche Diagnostics GmbH) release.

### *2.3.2 Cell activity*

Metabolic activity of SaOS-2 was assessed after 7 and 14 days of culture on material samples and CTR–. Cell proliferation was measured by WST1 (see method above). Supernatants were used for detecting the production of Alkaline Phosphatase, Type I Collagen, Tumor necrosis factor  $\alpha$  (ALP, COLL1, TNF $\alpha$  immunoenzymatic assay, USCN Life Science, Wuhan, China). Cell lysates were collected to measure activated Caspase-3 (Immunoenzymatic assay, Invitrogen Corp. CA, USA).



### 2.3.2 Statistical analysis

Statistical evaluation of data was performed using the software package SPSS/PC+Statistics™ 23.0 (SPSS Inc., Chicago, IL USA). The study is the results of three independent experiments and data are reported as mean  $\pm$  standard deviations (SD) at a significance level of  $p < 0.05$ . After having verified normal distribution and homogeneity of variance, a one-way ANOVA was done for comparison between groups. Finally, post hoc multiple comparison test (Dunnett) and correlation test (Pearson) were performed to detect significant differences among groups and controls.

## 3. Results and Discussion

### 3.1 Characterization of potassium (9R)-9-hydroxystearate

The inclusion of hydroxystearate anion (HSA) in hydroxyapatite required the conversion of the acid in a water soluble saline form. Both sodium- and potassium- (9R)-9-hydroxystearate were synthesized. However the sodium salt proved to be a particularly insoluble salt, whereas potassium salt proved to be more readily dissolved in water, especially once heated above 85 °C. The salification reaction of (9R)-9-hydroxystearic acid is reported in Figure S1. Potassium (9R)-9-hydroxystearate was characterized by  $^1\text{H}$  NMR, IR, and ESI Mass spectrometry and data obtained agree with the expected structure. In particular, ESI mass spectra were recorded both in  $\text{ESI}^+$  and  $\text{ESI}^-$  mode: the  $\text{ESI}^-$  spectrum (**Figure S1**) showed the peak at  $m/z = 299$ , corresponding to the molecular ion of the conjugate base of (9R)-9-HSA, and a lower peak at  $m/z = 149$  indicating the presence of a double salt, the doubly deprotonated form of 9-HSA; the  $\text{ESI}^+$  spectrum showed the mass of the potassium ion (**Figure S2**).

### 3.2 Characterization of the composite nanocrystals

The X-ray diffraction patterns of the solid products synthesized in the presence of 9R-HSA-K are consistent with the presence of hydroxyapatite as unique crystalline phase (**Figure 1**).

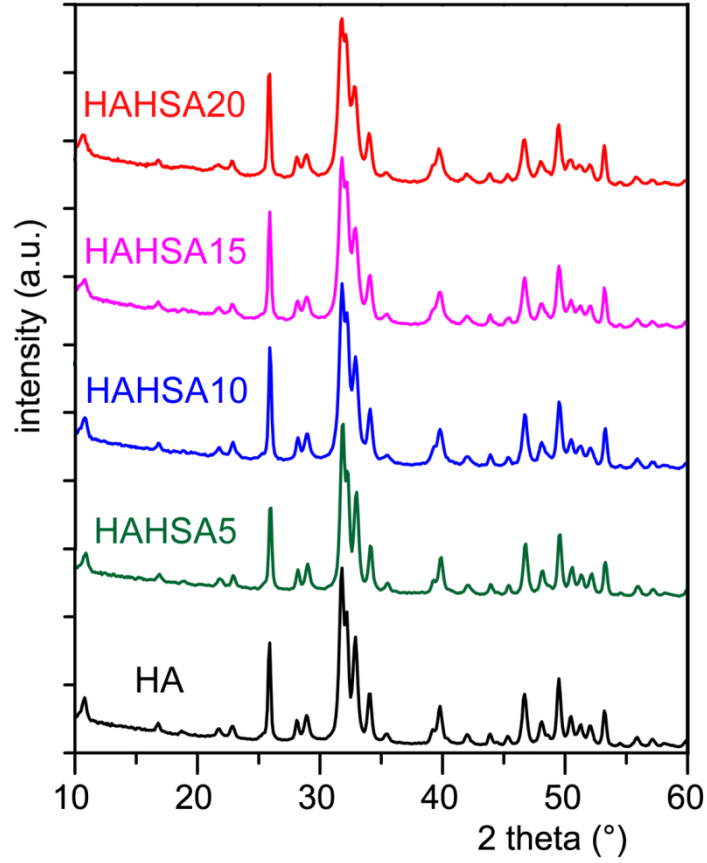


**Figure 1.** Powder X-ray diffraction patterns of the products synthesized in presence of different amounts of HSA.

Comparison of the patterns of the samples synthesized in the presence of increasing concentration of 9R-HSA-K shows an increase of the broadening of the diffraction peaks, which indicates a reduction the length of coherently scattering domains (i.e. the crystallite size) ( $\tau_{hkl}$ ). The values of  $\tau_{002}$ , which is related to the mean crystallite size along the *c*-axis, and of  $\tau_{310}$ , which refers to the mean crystallite size along a direction perpendicular to it, were calculated from the widths at half maximum intensity ( $\beta_{1/2}$ ) using the Scherrer equation on the hypothesis of negligible microstrain:<sup>18</sup>

$$\tau_{hkl} = k\lambda/\beta_{1/2}\cos\theta$$

where  $\lambda$  is the wavelength,  $\theta$  the diffraction angle and  $K$  a constant depending on crystal habit (chosen as 0.9). The silicon standard peak 111 was used to evaluate the instrumental broadening.

The data reported in **Table 1** show that the decrease of the length of the coherent scattering domains is not isotropic. In fact,  $\tau_{310}$  decreases on increasing 9R-HSA-K concentration in solution down by

about 30%, whereas the reduction of  $\tau_{002}$  amounts to just 17%, suggesting a preferential adsorption of hydroxystearate on HA crystal faces parallel to the  $c$ -axis direction, similarly to what previously reported for the interaction of acidic amino- and polyamino-acids with HA.<sup>5,16,19,20</sup>

**Table 1.** Coherent lengths ( $\tau_{hkl}$ ) of the perfect crystalline domains in the direction normal to 002 and to 310 planes calculated using the Scherrer method and lattice parameters calculated using the Rietveld method.

Samples	$\tau_{002}$ (Å)	$\tau_{310}$ (Å)	$a$ (Å)	$c$ (Å)	Unit cell volume (Å <sup>3</sup> )
HA	586 (7)	223 (2)	9.422 (2)	6.881 (2)	529.2 (1)
HAHSA5	550 (5)	218 (2)	9.426 (3)	6.883 (2)	529.7 (3)
HAHSA10	536 (6)	194 (2)	9.431 (2)	6.880 (1)	529.8 (1)
HAHSA15	505 (4)	162 (2)	9.431 (2)	6.881 (3)	530.1 (3)
HAHSA20	488 (4)	156 (1)	9.430 (1)	6.880 (2)	529.8 (2)

At variance, in spite of the slight increase of the  $a$ -axis dimension with composition, the incorporation of HSA does not significantly influence the cell volume of HA (Table 1). This is not surprising when considering the relative great dimensions of HSA, which should hinder its incorporation within hydroxyapatite crystal lattice whereas it is not an obstacle to its adsorption onto HA crystals. A preferential adsorption onto the HA faces parallel to the  $c$ -axis is further supported by the results of TEM investigation. TEM images of the different products show that they are constituted of rod-like crystals, coherently with the typical morphology of HA, which is characterized by crystals elongated along the  $c$ -axis direction. However, the dimensions of the nanocrystals decrease significantly on increasing hydroxystearate concentration, as shown in **Figure 2**.

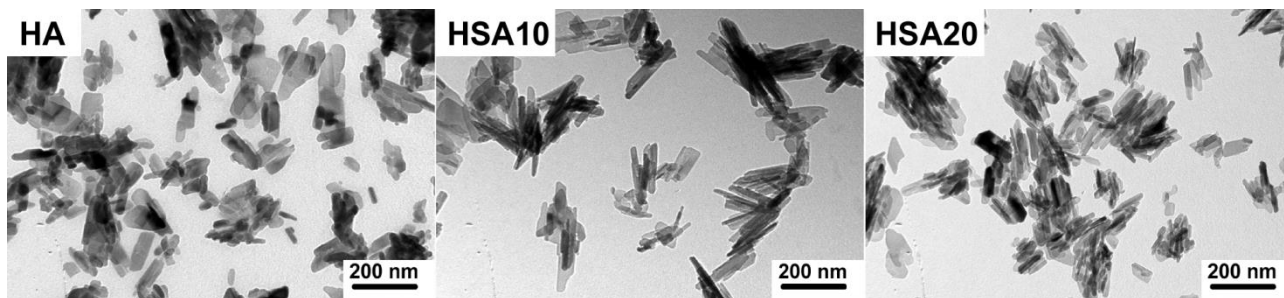


**Figure 2.** TEM images of HA, HAHSA10, and HAHSA20 nanocrystals.

The evaluation of the crystal dimensions shows that the reduction is not uniform, since the length and the width of the crystals decrease from about 215 to 70 nm and from about 65 to 15 nm respectively, on passing from HA to HAHS20, which means an increase of the length/width ratio from about 3.3 to about 4.7. The observed dimensional variations have a minor effect on the surface area: the values of SSA of the hydroxystearic containing samples appear reduced with respect to that of HA, but they do not exhibit significant variation as a function of composition (**Table 2**).

**Table 2.** HSA content, zeta potential, specific surface area and contact angle values of solid samples synthesized in the presence of different concentrations of HSA in solution.

Samples	HSA content (wt%)	Zeta potential (mV)	SSA (m <sup>2</sup> gr <sup>-1</sup> )	Contact angle (°)
HA	---	-12.5	56	7
HAHSA5	2.1	-17.8	48	69
HAHSA10	4.4	-19.0	42	91
HAHSA15	6.5	-20.4	48	93
HAHSA20	8.6	-20.6	50	92

The quantitative amount of HSA adsorbed onto HA nanocrystals has been determined through thermogravimetric analysis, by exploiting the fact that hydroxystearate decomposes completely between 200 and 600°C (**Figure S3**). The thermogravimetric plots reported in **Figure 3a** show that the total weight loss of the different samples increases on increasing 9R-HSA-K concentration in solution. Hydroxystearate content in the solid products, evaluated as the difference between the total weight loss of the sample and that of HA, increases linearly with concentration up to about 8.6 wt% (Table 2, Figure 3b).

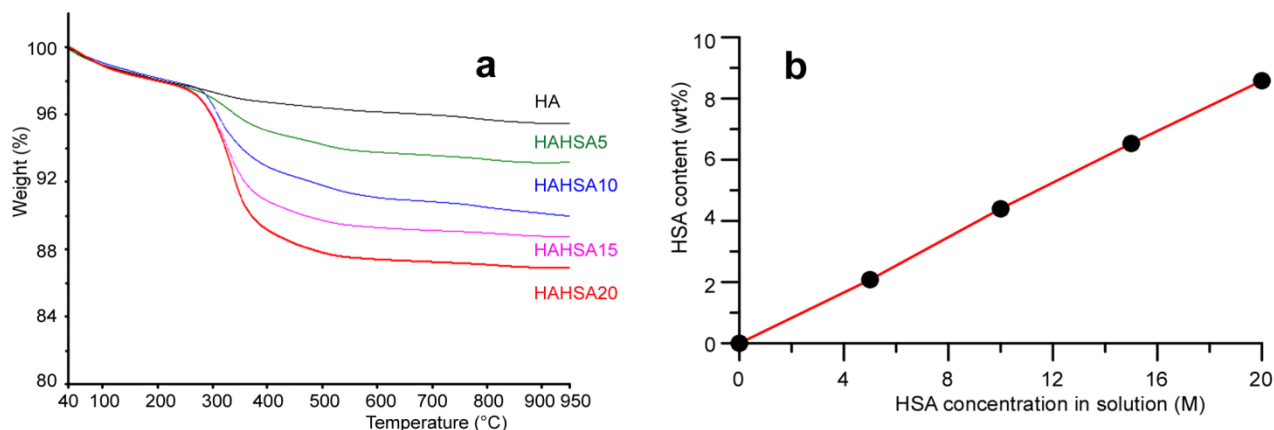


**Figure 3.** (a) Thermogravimetric plots of the products synthesized in presence of different amounts of HSA. (b) Hydroxystearate content in the different samples, evaluated through thermogravimetric analysis, as a function HSA concentration in solution.

The presence of HSA in the composite nanocrystals can be appreciated also on the infrared spectra of the different samples. **Figure 4** reports the infrared spectra of the products synthesized in presence of different concentration of 9R-HSA-K compared with that of HA. The spectra of the composite nanocrystals show the characteristic absorption bands of hydroxyapatite, together with absorption bands at 2923 and 2850  $\text{cm}^{-1}$ , corresponding to C-H stretching mode, and at 1558  $\text{cm}^{-1}$ , due to the asymmetric stretching mode of the carboxylate anion. Further absorption bands in the range 1470-1420  $\text{cm}^{-1}$ , due to the overlapping of the symmetric stretching mode of the carboxylate anion with the bending mode of the  $\text{CH}_2$  groups are also detectable. All these bands are clearly appreciable in the spectrum of 9R-HSA-K, which is compared with that of (9R)-9-HSA in **Figure S4**.

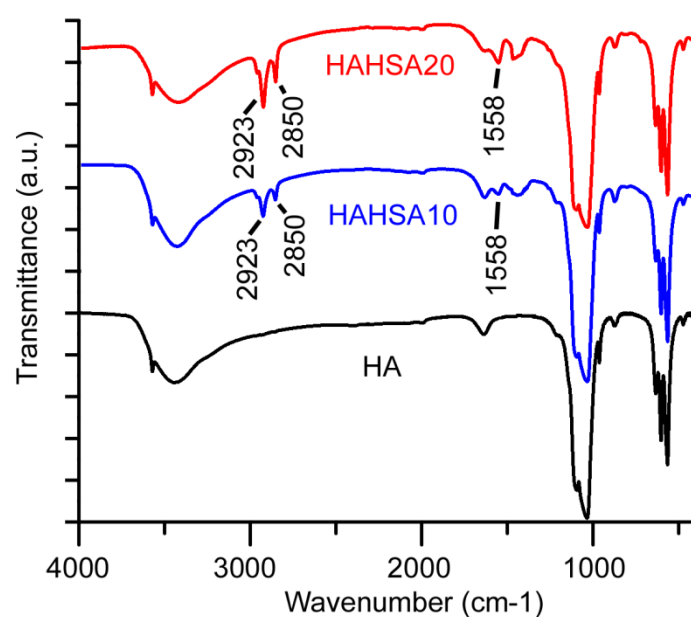


**Figure 4.** FTIR spectra of HA, HAHSA10, and HAHSA20.

In agreement with the hydrophilic character of hydroxyapatite, the value of contact angle measured onto HA is very low, just 7° measured after 0.33 s the water droplet contacted the surface, whereas water was completely spread on the surface after 4 s. The presence of hydroxystearate in the

composite nanocrystals provokes a remarkable increase in values of the contact angle, up to 69° onto HA/HSA5 and around 90° onto the samples at greater HSA content (Table 2), which remain constant during the 30 s of acquisition. It is reasonable to suppose that the increase of contact angle is due to the presence of the hydrophobic tails of HSA on the surface of the materials, whereas the charged carboxylate heads interact with calcium ions of HA. This interaction should reduce the ratio between Ca<sup>2+</sup>-rich sites and phosphate-rich sites, making the surface of HA more negative, with a consequent decrease of zeta potential.<sup>21</sup> Indeed, the composite nanocrystals exhibit more negative values of zeta potential with respect to that measured for HA, as shown in Table 2.

### **3.3 *In vitro* study**

SaOS2 is an osteosarcoma cell line useful model for testing biomaterials,<sup>22</sup> with good responsiveness in *in vitro* studies of cell-material interaction. SaOS2 are well characterized and exhibit osteoblastic properties, including the ability to produce the most common markers of osteoblast differentiation, such as the proteins of the extracellular matrix, and mineralization. As with all cell lines, there are some differences with respect to primary cells, which need to be considered when interpreting experimental data. However, they are widely used for *in vitro* tests for easy availability and maintenance, and reliable reproducibility. In the present study SaOS2 were cultured directly onto hydroxyapatite samples at different hydroxystearate content, in order to verify if HSA has a cytostatic and cytotoxic effect even if incorporated in HA nanocrystals.

#### **3.3.1 Cytotoxicity tests**

WST1 assay results at 3 days of culture are reported in **Figure 5a**. The viability of each experimental group, calculated as percentage of CTR– (100%), is also reported in the figure.

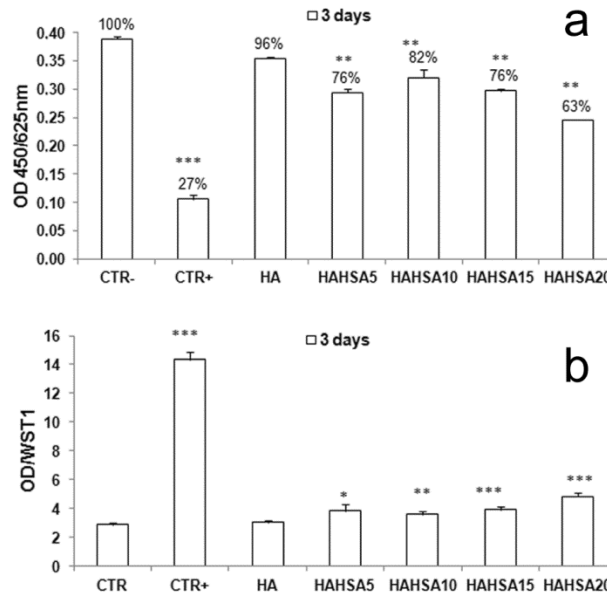


**Figure 5.** WST1 assay (a), and LDH release (b) of SaOS2 after 3 days of culture on HA, HSA samples, and CTRs. Values are reported as mean  $\pm$  SD (\* $p < 0.05$ ; \*\* $p < 0.005$ ; \*\*\* $p < 0.0005$ ).

- CTR-, HA vs HAHA5, HAHA10, HAHA15, HAHA20  $p < 0.005$ ; CTR+ vs ALL GROUPS  $p < 0.0005$ .
- CTR vs HAHA5  $p < 0.05$ ; HAHA10  $p < 0.005$ ; HAHA15, HAHA20  $p < 0.0005$ ; HA vs HAHA10  $p < 0.005$ ; HAHA15, HAHA20  $p < 0.0005$ ; CTR+ vs ALL GROUPS  $p < 0.0005$ .

A viability value under 70% is considered as a significant result of cytotoxic effect on SaOS2.<sup>17</sup> At 3 days only HAHA20 showed a 63% viability in comparison with CTR-, even if the statistical analysis using post hoc test to detect differences among groups revealed that cell proliferation on HAHA samples were significantly lower when compared to CTR- and to reference HA. The decrease of cell viability due to the effects of HSA was linked to cytotoxic effect revealed by LDH assay (**Figure 5b**). LDH release is an index of cytotoxic action, because this intracellular enzyme is found in supernatant as a consequence of cytoplasmatic membrane damage.<sup>23</sup> LDH was detected in culture medium at 3 days and its measure showed that HAHA groups had significant higher values than CTR- (from HAHA5 to HAHA20) and HA (HAHA10, HAHA15, HAHA20). As expected, CTR+ showed the significant highest value.

### 3.3.2 Cells proliferation and metabolic activity.

WST1 assay results at 7 and 14 days of culture are reported in **Figure 6a**. At 7 and 14 days values of all experimental groups dramatically decreased (below 60% and below 30% respectively) when compared to both CTR and HA groups.

The decrease of cell viability due to the presence of HSA was evaluated by other parameters linked to cytotoxicity, such as TNF $\alpha$  and Caspase-3 (**Figure 6b-c**). Cytotoxicity tests results were also confirmed by TNF $\alpha$  level, whose production was significantly elevated in all HAHSA groups, both at 7 and at 14 days, when compared to CTR and HA. TNF $\alpha$  is a mediator of inflammation and it is also involved in apoptotic cell death.<sup>24</sup> 9-HSA is known to induce apoptosis in osteosarcoma cells through a mitochondrial pathway, with an increase of Caspase-9 activity.<sup>12</sup> The results obtained on the activation of Caspase-3, that interacts with Caspase-9 in the same pathway, showed that active Caspase-3 from HAHSA10 to HAHSA20 groups was significantly higher than CTR, HA and HAHSA5 groups. Statistical analysis (Pearson correlation test) demonstrated that results of LDH, TNF $\alpha$  and Caspase-3 were consistent and inversely correlated to WST1 proliferation assay. Data showed that the presence of HSA in the composite HA nanocrystals has antiproliferative effects and induces cytotoxicity, according to a dose-response effect.



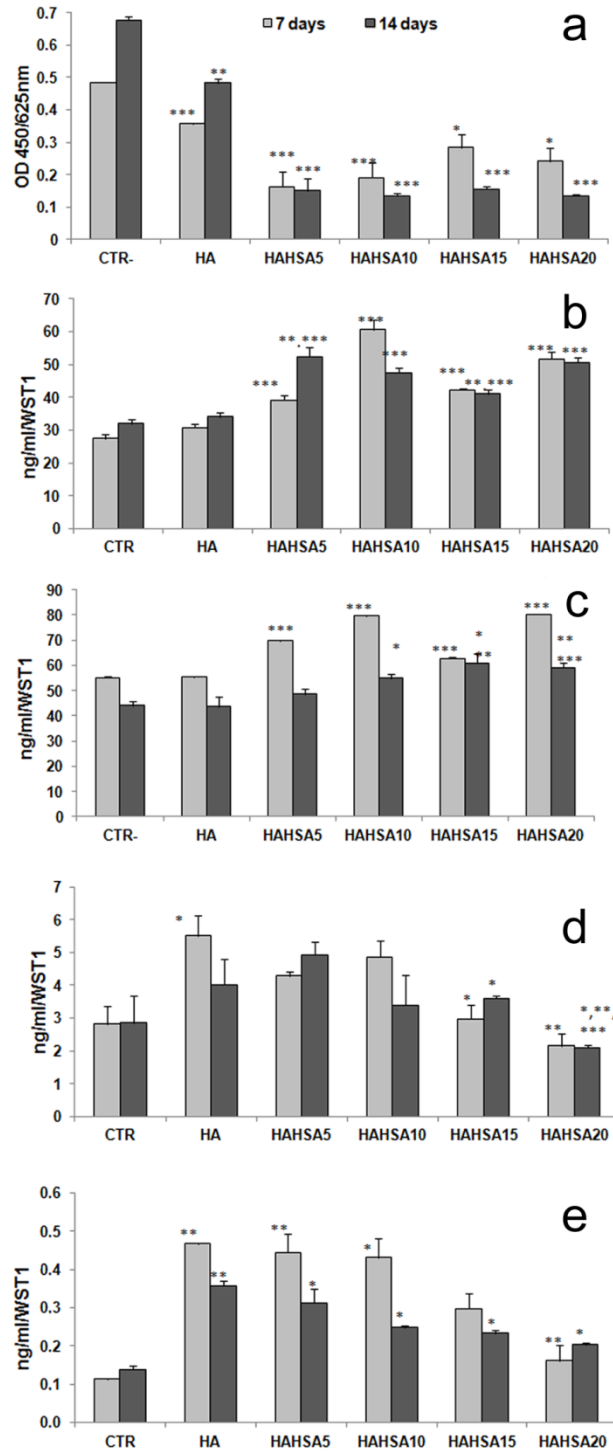


**Figure 6.** WST1 assay (a), TNFα (b), Caspase 3 (c), ALP (d) and COLL1 (e) measured in SaOS-2 after 7 and 14 days of culture on HA, HSA samples and CTR. Values are reported as mean ± SD (\*p<0.05; \*\*p<0.005; \*\*\*p<0.0005). Pearson correlation test: LDH/Caspase: 0.787 (p<0.0005); LDH/TNFα: 0.495 (p<0.05); Caspase-3/TNFα :0.524 (p<0.05); WST1/LDH, Caspase-3, TNFα: -0.899, -0.791, -0.949 respectively (p<0.0005)

- a. 7 days: CTR vs HA  $p < 0.0005$ ; CTR, HA vs HAHA5, HAHA10  $p < 0.0005$ ; CTR, HA vs HAHA15, HAHA20  $p < 0.05$ . 14 days: CTR vs HA  $p < 0.005$ ; CTR, HA vs HAHA5, HAHA10, HAHA15, HAHA20  $p < 0.0005$
- b. 7 days: CTR, HA vs HAHA5, HAHA10, HAHA15, HAHA20  $p < 0.0005$ ; 14 days: CTR vs HAHA5, HAHA10, HAHA15, HAHA20  $p < 0.0005$ ; HA vs HAHA5, HAHA15  $p < 0.005$ , HAHA10, HAHA20  $p < 0.0005$ .
- c. 7 days: CTR, HA vs HAHA5, HAHA10, HAHA15, HAHA20  $p < 0.0005$ ; 14 days: HAHA10 vs CTR  $p < 0.0005$ , HA, HAHA5  $p < 0.05$ ; HAHA15 vs CTR, HA  $p < 0.005$ , HAHA5  $p < 0.05$ ; HAHA20 vs CTR  $p < 0.0005$ , HA, HAHA5  $p < 0.005$ .
- d. 7 days: HA vs CTR  $p < 0.05$ ; HAHA15 vs HA, HAHA5, HAHA10  $p < 0.05$ ; HAHA20 vs HA, HAHA5, HAHA10  $p < 0.005$ ; 14 days: HAHA15 vs HA, HAHA5,  $p < 0.05$ ; HAHA20 vs HA, HAHA5, HAHA10  $p < 0.005$ ; HAHA20 vs HA  $p < 0.05$ , HAHA5  $p < 0.005$ , HAHA15  $p < 0.0005$
- e. 7 days: CTR vs HA, HAHA5  $p < 0.005$ , HAHA10  $p < 0.05$ ; HA vs HAHA20  $p < 0.005$ ; 14 days: CTR vs HA  $p < 0.005$ , HAHA5  $p < 0.05$ ; HA vs HAHA10, HAHA15, HAHA20  $p < 0.05$

Metabolic activity of SaOS-2 was explored at 7 and 14 days by measuring Alkaline Phosphatase and Collagen type1 as markers of extracellular matrix synthesized by differentiated osteoblasts.<sup>25-28</sup> Cells grown in direct contact with HA demonstrated a differentiated state, with significant higher values of ALP and COL1 with respect to CTR (**Figure 6 d-e**). The presence of HSA influenced SaOS-2 behavior: HAHA15 and HAHA20 showed a significant reduction of ALP activity when compared to HA. ALP level of HAHA15 and HAHA20 groups was also lower than HAHA5 at both experimental times. COL1 production of HAHA10, HAHA15 (14 days), and HAHA20 (7 and 14 days) was significantly lower than that of HA. SaOS-2 cultured on HAHA5 at 7 and 14 days, HAHA10 and HAHA15 at 7 days did not show altered production of COL1.

Despite the high level of cytotoxicity parameters previously described, HAHA5 and, at least partially, HAHA10 showed a good expression of extracellular matrix markers, exhibiting a behavior similar to HA group with regard to ALP and COL1 production. It seems that even if a significant high percentage of SaOS-2 was dead or in a apoptotic state, a little part of cells were still alive and active when cultured at relatively low HSA content in the composite nanocrystals. The presence of higher contents (about 6.5 and 8.6 wt% in HAHA15 and HAHA20, respectively) inhibited the responsiveness of SaOS-2: most of cells were died or apoptotic, whereas alive cells were not active, but probably quiescent in the early G0/G1 cell cycle, as also reported in literature.<sup>12</sup>

#### **4. Conclusions**

The use of the potassium salt of (9R)-9-hydroxystearic acid proved to be a good strategy to functionalize HA with increasing amounts of hydroxystearate up to about 8.6 wt%. The preferential adsorption onto specific HA crystal faces modulates the crystallinity and morphology of the composite nanocrystals. The synthesized new materials are able to dramatically affect proliferation, viability and activity of SaOS2 osteosarcoma cell line. In particular, all the samples displayed significantly reduced viability with respect to pure HA and a dose dependent effect on cytotoxicity parameters, suggesting that these materials could be usefully applied at specific bone sites for the local treatment of bone metastases.

**Supporting Information:** Experimental: Synthesis of (9R)-9-hydroxystearic acid; Experimental: Characterization of composite samples; Figures S1 to S5.

#### **Acknowledgements**

This research was carried out with the financial support of University of Bologna (FARB 2012). This work was partially supported by the Italian Programme of Donation for Research “5 per mille” Italian Health Ministry, year 2012, Rizzoli Orthopaedic Institute. The authors thank Dr. Katia Rubini, Ms.

Luiza Mamigonian Bessa and the EU for providing a scholarship through the “Advanced Spectroscopy in Chemistry” Erasmus Mundus European Master Programme.

## Notes

The authors declare no competing financial interests

## References

- (1) Chai, Y.C.; Carlier, A.; Bolander, J.; Roberts, S.J.; Geris, L.; Schrooten, J.; Van Oosterwyck, H.; Luyten, F.P.; Current views on calcium phosphate osteogenicity and the translation into effective bone regeneration strategies, *Acta Biomater*, **2012**, 8, 3876–3887.
- (2) Dorozhkin, S.V.; Self-setting calcium orthophosphate formulations, *J Funct Biomater*, **2013**, 4, 209–311.
- (3) Surmenev, R. A.; Surmeneva, M. A.; Ivanova, A. A. Significance of calcium phosphate coatings for the enhancement of newbone osteogenesis – A review. *Acta Biomater*. **2014**, 10, 557–579.
- (4) Shimomura, K.; Moriguchi, Y.; Murawski, C. D.; Yoshikawa, H.; Nakamura, N. Osteochondral tissue engineering with biphasic scaffold: current strategies and techniques. *Tissue Eng. Part B* **2014**, 20, 468–476.
- (5) Boanini, E.; Torricelli, P.; Gazzano M.; Giardino R.; Bigi A. Nanocomposites of hydroxyapatite with aspartic acid and glutamic acid and their interaction with osteoblast-like cells. *Biomaterials* **2006**, 27, 4428–4433.
- (6) Kyllönen, L.; D’Este, M.; Alini, M.; Eglin, D. Local drug delivery for enhancing fracture healing in osteoporotic bone. *Acta Biomater*. **2015**, 11, 412–434.
- (7) Queffélec, C.; Petit, M.; Janvier, P.; Knight, D. A.; Bujoli, B. Surface modification using phosphonic acids and esters. *Chem. Rev.* **2012**, 112, 3777–3807.

- (8) Weidner, T.; Dubey, M.; Breen, N. F.; Ash, J.; Baio, J. E.; Jaye, C.; Fischer, D. A.; Drobny, G. P.; Castner, D. G. Direct observation of phenylalanine orientations in statherin bound to hydroxyapatite surfaces. *J. Am. Chem. Soc.* **2012**, *134*, 8750–8753
- (9) Masotti, L.; Casali, E.; Gesmundo, N.; Sartor, G.; Galeotti, T.; Borrello, S.; Piretti, M.; Pagliuca, G. Lipid peroxidation in cancer cells: chemical and physical studies. *Ann. NY Acad. Sci.* **1988**, *551*, 47–58.
- (10) Calonghi, N.; Cappadone, C.; Pagnotta, E.; Boga, C.; Bertucci, C.; Fiori, J.; Tasco, G.L.; Casadio, R.; Masotti, L. Histone deacetylase 1: a target of 9-hydroxystearic acid in the inhibition of cell growth in human colon cancer. *J. Lipid Res.* **2005**, *46*, 1596–1603.
- (11) Juan, L. J.; Shia, W. J.; Chen, M. H.; Yang, W. M.; Seto, E.; Lin, Y. S.; Wu, C. W. Histone deacetylases specifically down-regulate p53-dependent gene activation, *J. Biol. Chem.* **2000**, *275*, 20436–20443.
- (12) Calonghi, N.; Pagnotta, E.; Parolin, C.; Molinari, C.; Boga, C.; Dal Piaz, F.; Brusa, G.L.; Santucci, M.A.; Masotti, L. Modulation of apoptotic signalling by 9-hydroxystearic acid in osteosarcoma cells. *Biochim. Biophys. Acta* **2007**, *1771*, 139–146.
- (13) Parolin, C.; Calonghi, N.; Presta, E.; Boga, C.; Caruana, P.; Naldi, M.; Andrisano, V.; Masotti, L.; Sartor, G. Mechanism and stereoselectivity of HDAC I inhibition by (R)-9-hydroxystearic acid in colon cancer. *Biochim. Biophys. Acta* **2012**, *1821*, 1334–1340.
- (14) Binder, R. G.; Applewhite, T. H.; Diamond, M. J.; Goldblatt, L. A. Chromatographic analysis of seed oils. II. Fatty acid composition of *Dimorphotheca* oil. *J. Am. Oil Chem. Soc.* **1964**, *41*, 108–111.
- (15) Ebert, C.; Felluga, F.; Forzato, C.; Foscatto, M.; Gardossi, L.; Nitti, P.; Pitacco, G.; Boga, C.; Caruana, P.; Micheletti, G.; Calonghi, N.; Masotti, L. Enzymatic kinetic resolution of hydroxystearic acids: A combined experimental and molecular modelling investigation. *J. Mol. Catal. B: Enzym.* **2012**, *83*, 38–45.

- (16) Bigi, A.; Boanini, E.; Gazzano, M.; Kojdecki, M. A.; Rubini, K. Microstructural investigation of hydroxyapatite–polyelectrolyte composites. *J. Mater. Chem.* **2004**, *14*, 274–279.
- (17) UNI EN ISO 10993-5, Biological evaluation of medical devices – Part 5. Tests for in vitro cytotoxicity.
- (18) Klug, H. P.; Alexander, L. E. *X-ray diffraction procedures for polycrystalline and amorphous materials*; Wiley-Interscience: New York, 1974.
- (19) Gonzalez-McQuire, R.; Chane-Ching, J. Y.; Vignaud, E.; Lebugle, A.; Mann S. Synthesis and characterization of amino acid-functionalized hydroxyapatite nanorods. *J. Mater. Chem.* **2004**, *14*, 2277–2281.
- (20) Almora-Barrios, N.; Austen, K. F.; de Leeuw, N. H. Density functional theory study of the binding of glycine, proline, and hydroxyproline to the hydroxyapatite (0001) and (0110) surfaces. *Langmuir* **2009**, *25*, 5018-5025.
- (21) Boanini, E.; Gazzano, M.; Bigi, A. Time course of zoledronate interaction with hydroxyapatite nanocrystals. *J. Phys. Chem. C* **2012**, *116*, 15812–15818.
- (22) Czekanska, E. M.; Stoddart, M. J.; Richards, R. G.; Hayes, J. S. In search of an osteoblast cell model for in vitro research. *Eur. Cell. Mater.* **2012**, *24*, 1–17.
- (23) Gori, F.; Hofbauer, L. C.; Dunstan, C. R.; Spelberg, T. C.; Khosla, S.; Riggs, B. L. The expression of Osteoprotegerin and Rank ligand and the support of osteoclast formation by stromal-osteoblast lineage cells is developmentally regulated. *Endocrinology* **2000**, *141*, 4768-4776.
- (24) MacEwan, D. J. TNF ligands and receptors – a matter of life and death. *Br. J. Pharmacol.* **2002**, *135*, 855-875.
- (25) Malaval, L.; Liu, F.; Roche, P.; Aubin, J. E. Kinetics of osteoprogenitor proliferation and osteoblast differentiation in vitro. *J. Cell. Biochem.* **1999**, *74*, 616-627.
- (26) Atsushi, E.; Korenori, O.; Satoshi, I.; Shigeyuki, E.; Takayoshi, N.; Yukichi, U. Effects of  $\alpha$ -TCP and TetCP on MC3T3-E1 proliferation, differentiation and mineralization. *Biomaterials* **2003**, *24*, 831-836.

- (27) Franceschi, R.T.; Iyer, B.S.; Relationship between collagen synthesis and expression of the osteoblast phenotype in MC3T3-E1 cells. *J. Bone Miner. Res.* **1992**, 7, 235-46.
- (28) Cowles, E. A.; DeRome, D.; Pastizzo, G.; Brailey, L. L.; Gronowicz, G. A. Mineralization and the expression of matrix proteins during in vivo bone development. *Calcif. Tissue Int.* **1998**, 62, 74-82.

## Table of Contents Graphic

